2005-01-3735

Enthalpy-Based Flamelet Model for HCCI Applied to a Rapid Compression Machine

David J. Cook* & Heinz Pitsch

Department of Mechanical Engeering, Stanford University, Stanford, California 94305

ABSTRACT

Homogeneous-Charge Compression Ignition (HCCI) engines have been shown to have higher thermal efficiencies and lower NO_x and soot emissions than Spark Ignition engines. However, HCCI engines experience high levels of carbon monoxide (CO) and unburnt hydrocarbon (UHC) emissions. These pollutants are formed in regions of the cylinder where wall heat loss is significant. Improving CO and UHC emissions in HCCI engines requires a fundamental understanding of the heat loss, chemical kinetics, and transport between near wall regions and regions less affected by heat loss. In this study an enthalpy-based flamelet approach is introduced and applied in a simulation of a Rapid Compression Machine operated under HCCI conditions. This approach directly models transport between regions of higher and lower enthalpies. Results are compared to experimental data from Murase and Hanada [6]. The simulations correctly predict ignition timing trends as a function of initial mixture temperature. Additionally, the affect of modeled transport across enthalpies on ignition characteristics is quantified. It is demonstrated that this term is important and is of comparable magnitude to the chemical source term.

INTRODUCTION

Homogeneous-Charge Compression Ignition (HCCI) engines have recently been the subject of much research effort for both their low NO_x (oxides of nitrogen) and soot emissions, and higher thermal efficiency compared to Spark Ignition (SI) engines. While significant progress has been made, these engines continue to suffer from high carbon monoxide (CO) and unburnt hydrocarbon (UHC) emissions. Before HCCI engines can become commercially feasible, CO and UHC emissions must be reduced. As experimental data suggests that cylinder flow and turbulence play an important role in HCCI combustion [1], a better understanding of its interaction with chemical kinetics could be used to reduce CO and UHC emissions in HCCI engines.

The relatively high CO emissions in HCCI engines are a consequence of the strategy used to achieve the main goal of reducing NO_x . Experimentally, it has been found that CO emissions originate in regions where the gas temperature does not exceed 1500 K [2]. Yet, in order to create low NO_x emissions, HCCI engines are run with low peak temperatures. This is generally accomplished by running the engines very lean or, more commonly, highly diluted with significant internal or external Exhaust Gas Recirculation (EGR). Such operating strategies result in a maximum burnt gas temperature below 1850 K, and therefore lead to low NO_x emissions. Having a maximum burnt gas temperature below 1850 K in the cylinder implies that in regions strongly affected by wall heat loss, conditions favorable for producing higher CO emissions will occur.

Unburnt hydrocarbon emissions come from regions in the cylinder where auto-ignition does not occur. These regions are typically either extremely dilute (as in the case of a partially stratified charge from direct injection), or are affected by wall heat loss, or both. Another major cause of UHC emissions is cycles in which misfire occurs. However, as control of ignition timing in HCCI engines improves, this

*Email: david.cook@stanford.edu

cause of UHC emissions is likely to become less significant.

Thus, wall heat loss effects are a common cause of both CO and UHC emissions in HCCI engines. While HCCI refers to a type of combustion which typically has a homogeneous charge in terms of mixture composition, the charge experiences large stratification in the enthalpy field due to wall heat loss or heating because of hot valves. This stratification typically causes regions in the center of the cylinder to ignite first, followed later by regions closer to the cylinder walls. These effects have been modeled using multiple zones, where ignition of gas with a smaller enthalpy defect (i.e. gases less effected by wall heat loss) affects gases with higher levels of enthalpy defect only through the increased pressure associated with the volumetric expansion of the ignited gases [3]. Additionally, fully coupled CFD and chemistry studies have been done in which the chemical source terms have been evaluated using mean values and utilizing a low-order correction for the effects of turbulence in the combustion process [4].

In this study, the effect of wall heat transfer on combustion is modeled using a flamelet-type approach. In this model, flamelet equations are formulated in a normalized enthalpy space. Transport across this enthalpy space physically represents the interaction between gases of higher and lower levels of enthalpy defect.

ENTHALPY-BASED FLAMELET MODELING

In this section, a derivation of the enthalpy-based flamelet equations will be given. The general equations for species mass-fraction transport and total enthalpy transport are as follows

$$\rho\frac{\partial Y_i}{\partial t}+\rho v_j\frac{\partial Y_i}{\partial x_j} = \frac{\partial}{\partial x_j}\left(\rho D\frac{\partial Y_i}{\partial x_j}\right)+\rho\dot{\omega}_i \quad (1)$$

$$\rho\frac{\partial H}{\partial t}+\rho v_j\frac{\partial H}{\partial x_j} = \frac{\partial}{\partial x_j}\left(\rho D\frac{\partial H}{\partial x_j}\right)+\left(\frac{\partial p}{\partial t}-\dot{q}_{\Delta \mathrm{h}}\right), \quad (2)$$

where Y_i is mass fraction of species i, H is total enthalpy, ρ is density, D is molecular diffusivity, $\dot{\omega}_i$ is the chemical source term for species i, p is pressure, $\dot{q}_{\Delta \mathrm{h}}$ accounts for volumetric heat loss such as radiation, and v_j is velocity in the x_j direction. The (x_1, x_2, x_3)-coordinate system can be transformed into a a system which locally aligns with the enthalpy gradients. In the following analysis of this transformation, the x_1-coordinate is assumed to be normal and the x_2 and x_3-coordinates are assumed to be tangential to an iso-value surface of enthalpy. This transformation is made such that

$$(t, x_1, x_2, x_3) \rightarrow (\tau, H, H_2, H_3), \quad (3)$$

where enthalpy is introduced as a new independent coordinate. This implies that the new independent coordinate, H, is attached to an iso-surface of enthalpy and that the new coordinates H_2 and H_3 lie within this surface. Hence this transformation in space and in time coordinates is defined as

$$\frac{\partial}{\partial t} = \frac{\partial}{\partial \tau}+\frac{\partial H}{\partial t}\frac{\partial}{\partial H} \quad (4)$$

$$\nabla = \nabla H\frac{\partial}{\partial H}+\nabla_{H_\perp}, \text{ with } \nabla_{H_\perp}=\begin{pmatrix}0\\ \partial/\partial H_2\\ \partial/\partial H_3\end{pmatrix}. \quad (5)$$

If the gradients in the H-coordinate are assumed to be large compared to gradients in the H_2 and H_3 directions, which will be discussed in more detail below, then an asymptotic analysis similar to the one used by Peters (2000) [12] for the mixture fraction formulation of the flamelet equations can be applied. After such analysis, it can be shown that terms in the flamelet equations which include gradients in the H_2 and H_3 directions are small compared to other terms and therefore can be neglected. When this is done, the transformation of temporal and spatial derivatives is given by,

$$\frac{\partial}{\partial t} = \frac{\partial}{\partial \tau}+\frac{\partial H}{\partial t}\frac{\partial}{\partial H}, \quad (6)$$

$$\frac{\partial}{\partial x_j} = \frac{\partial H}{\partial x_j}\frac{\partial}{\partial H}. \quad (7)$$

Above, the fundamental assumption that the gradients in the H-direction are large compared to gradients in the H_2 and H_3 directions has been used. This assumption requires further discussion. The following arguments are presented for systems with inhomogeneities in enthalpy, but with initially perfect homogeneous mixture composition.

Chemical reactions in combustion systems are governed by Arrhenius rate expressions in which the reaction rates have an exponential dependence on temperature. Prior to ignition total enthalpies are directly related to temperature through specific heat. Therefore, reaction rates will also exhibit an exponential dependence on total enthalpy. Because of this, pre-ignition chemical kinetics and therefore the advancement of unburnt gas toward ignition will mostly align with the enthalpy field. From this analysis, we conclude that variations of species concentrations and temperature in the H-coordinate prior to ignition will be large compared to variations in the H_2 and H_3 directions. Therefore, prior to ignition, $\nabla_{H_\perp}$ is small compared to $\frac{\partial}{\partial H}$.

After the ignition of gases at higher enthalpies, large spatial gradients of species concentrations and temperature will exist between the unburnt and the ignited gases. Chemistry will then tend to be most active in small layers between unburnt and already ignited mixtures where thermal and species transport is large due to large local gradients. Transport across the small layers of most active chemistry in this case will mainly align with the enthalpy gradients and diffusion normal to the enthalpy gradients will be smaller. The flamelet assumption is valid for this case so long as the width of the thin layer is smaller than the smallest length scale of the turbulence.

In the case of small gradients the above assumption is not satisfied. However, in that case, diffusion is slow com-

pared to chemistry and therefore combustion during ignition approximates a series of homogeneous reactors. Hawkes et al. [9] conducted a Direct Numerical Simulation of two-dimensional turbulence with detailed hydrogen/air chemistry. For the cases with small fluctuations in unburnt temperature the use of a multizone model, in which diffusive transport affects were not included, led to good agreement with the DNS data. For this case of small enthalpy gradients, they showed that the chemical source term was the dominant term and that affects of diffusive transport were comparatively negligible. Therefore, diffusion is negligible entirely and the exclusion of the $\nabla_{H_\perp}$ term in the coordinate transformation will result in only negligible errors. Hence, for both cases of large and small gradients the $\nabla_{H_\perp}$ term is neglected in this study.

Applying Eq. (7) to Eq. (1) results in

$$\begin{aligned} \rho\frac{\partial Y_i}{\partial \tau} = & - \frac{\partial Y_i}{\partial H}\left(\rho\frac{\partial H}{\partial t} + \rho v_j \frac{\partial H}{\partial x_j}\right) \\ & + \frac{\partial Y_i}{\partial H}\left(\frac{\partial}{\partial x_j}\left(\rho D \frac{\partial H}{\partial x_j}\right)\right) \\ & + \rho D \frac{\partial H}{\partial x_j}\frac{\partial H}{\partial x_j}\frac{\partial^2 Y_i}{\partial H^2} + \rho\dot{\omega}_i \end{aligned} \tag{8}$$

Introducing a scalar dissipation rate in enthalpy-space, $\chi_{_H} \equiv 2D\frac{\partial H}{\partial x_j}\frac{\partial H}{\partial x_j}$, substituting Eq. (2) into Eq. (8), and canceling similar terms produces,

$$\rho\frac{\partial Y_i}{\partial \tau} + \left(\frac{\partial p}{\partial t} - \dot{q}_{\Delta \mathrm{h}}\right)\frac{\partial Y_i}{\partial H} = \frac{\rho\chi_{_H}}{2}\frac{\partial^2 Y_i}{\partial H^2} + \rho\dot{\omega}_i\,. \tag{9}$$

The second term on the left hand side represents a convection term in enthalpy space. This term is not present in the mixture fraction formulation of the flamelet equations, because mixture fraction is a conserved scalar, while enthalpy is not. The temperature equation can similarly be expressed in enthalpy space.

In order to simplify the numeric solution of the these equations, we normalize the enthalpy field and define a new coordinate ξ as

$$\xi = \frac{H - \Theta_{\min}(\tau)}{\Theta_{\max}(\tau) - \Theta_{\min}(\tau)} = \frac{H - \Theta_{\min}(\tau)}{\Delta\Theta(\tau)}\,. \tag{10}$$

$\Theta_{\min}(\tau)$ and $\Theta_{\max}(\tau)$ represent the minimum and maximum possible enthalpies in the system, as defined in the appendix (Eqs. 22 & 23), and therefore it can be shown that $0 \leq \xi \leq 1$.

Applying transformation derivatives, as defined in the appendix, and defining a normalized enthalpy dissipation rate ($\chi_{_\xi} = \chi_{_H}/(\Delta\Theta)^2$), we finally obtain the following form of the flamelet equations

$$\rho\frac{\partial Y_i}{\partial \tau^\star} = - \rho v_\xi \frac{\partial Y_i}{\partial \xi} + \frac{\rho\chi_\xi}{2}\frac{\partial^2 Y_i}{\partial \xi^2} + \rho\dot{\omega}_i\,, \tag{11}$$

$$\begin{aligned} \rho\frac{\partial T}{\partial \tau^\star} = & - \rho v_\xi \frac{\partial T}{\partial \xi} + \frac{\rho\chi_\xi}{2}\frac{\partial^2 T}{\partial \xi^2} \\ & + \frac{\rho\chi_\xi}{2C_p}\frac{\partial T}{\partial \xi}\left(\frac{\partial C_p}{\partial \xi} + \sum_i^{\mathrm{N}} c_{p,i}\frac{\partial Y_i}{\partial \xi}\right) \\ & - \frac{\rho}{C_p}\sum_i^{\mathrm{N}} h_i\dot{\omega}_i + \frac{1}{C_p}\left(\frac{\partial p}{\partial t} - \dot{q}_{\Delta h}\right)\,. \end{aligned} \tag{12}$$

Here C_p represents the specific heat of the mixture and v_ξ is the convective velocity in ξ-space as defined in the appendix by Eq. (34).

EXPERIMENT

To validate this approach, experimental results of auto-ignition in a Rapid Compression Machine (RCM) by Ref. [6] are used. The experiment involved an n-butane/air mixture with an equivalence ratio of 0.4, a compression ratio of 14.7, two different initial temperatures of 323 K and 333 K and pressure of 1 atm before compression. A fully premixed RCM experiment was chosen because the charge is fully homogeneous in mixture compositions while the charge has a stratified enthalpy field. Because of the contraction between the compression cylinder and combustion chamber in the experimental configuration, the charge gases experience large levels of thermal/enthalpy stratification. Therefore, this experiment is an example of a case where wall heat loss effects are particularly important.

CHEMICAL MECHANISM

A skeletal n-butane/air mechanism consisting of 119 species and 678 reactions was used in this study. The mechanism was based on a detailed chemical mechanism [7], which has been extensively validated for C7 and C8 hydrocarbon ignition, in which all C5 and higher species were eliminated. Additional species were reduced via a sensitivity analysis [8] for zero-dimensional auto-ignition of n-butane/air for equivalence ratios from 0.3 to 0.4 over a temperature range of 650-950 K. Over this range, the reduced mechanism agrees to within 2% with the ignition delay times given by the detailed chemical mechanism, and it agrees well with experimental data by Ref. [10].

MODELING APPROACH

A fully-implicit one-dimensional finite difference code was used to solve the combustion model, Eqs. (11) & (12). An equidistant grid of 101 points in ξ-space was used. The coupling of the flamelet code and CFD solver follows the

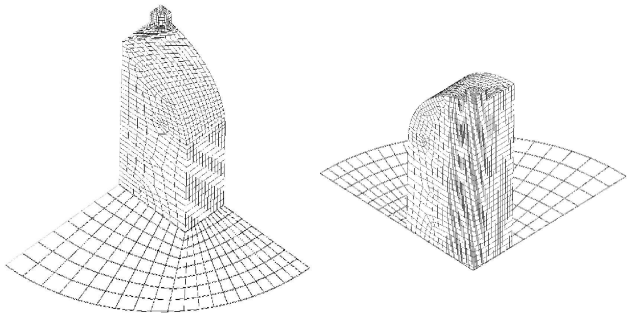

Figure 1: Computational domain.

Representative Interactive Flamelet (RIF) method for mixture fraction-based flamelet equations [11, 12, 13, 14].

Three-dimensional Navier-Stokes equations were solved using the commercial CFD software Fluent. The computational domain at top-dead-center is shown in Fig. 1. A zero-dimensional model was used to model blow-by, which must be included for accurate prediction of maximum pressures. Turbulence was modeled using the Renormalized Group (RNG) k–ϵ model. Additionally, the Favre averaged mean and variance equations for total enthalpy were solved, which are given as follows

$$\frac{\partial(\bar{\rho}\widetilde{H})}{\partial t} + \nabla\cdot\left[\bar{\rho}\tilde{\mathbf{u}}\widetilde{H}\right] = \nabla\cdot\left[\frac{\mu}{Sc_{\widetilde{H}}}\nabla\widetilde{H}\right] \quad (13)$$

$$\frac{\partial(\bar{\rho}\widetilde{H''^2})}{\partial t} + \nabla\cdot\left[\bar{\rho}\tilde{\mathbf{u}}\widetilde{H''^2}\right] = \nabla\cdot\left[\frac{\mu}{Sc_{\widetilde{H''^2}}}\nabla\widetilde{H''^2}\right] + \frac{2\mu}{\mathrm{Sc}_{\widetilde{H''^2}}}\left[\nabla\widetilde{H}\right]^2 - \bar{\rho}\widetilde{\chi}, \quad (14)$$

where $Sc_{\widetilde{H}}$ and $Sc_{\widetilde{H''^2}}$ are constants, tilde ($\tilde{}$) denotes Favre averaged quantities, which are functions of space and time, overline ($\bar{}$) denotes Reynolds averages, and hat ($\widehat{}$) denotes cylinder averaged quantities (Eq. 17), as used in the flamelet code.

For a mixture fraction formulation of the flamelet equations, the scalar dissipation rate is defined as $\chi \equiv 2D|\nabla Z|^2$, Ref. [12], which is often modeled as $\widetilde{\chi} = C_\chi\ (\tilde{\varepsilon}/\tilde{k})\ \widetilde{Z''^2}$ [15], where C_χ is a constant here taken to be 2 [15]. The latter of these equations illustrates its dependence on the variance of the mixture fraction and a characteristic turbulence time at the integral-scale, $\tilde{k}/\tilde{\varepsilon}$. In this study, these values are modeled analogously to the mixture fraction formulation, with $\widetilde{\chi} = C_\chi\ (\tilde{\varepsilon}/\tilde{k})\ \widetilde{H''^2}$ and a presumed ξ-functionality of the dissipation rate of the form

$$\chi(\xi) = \chi_{\mathrm{ref}}\left(\frac{\xi-\xi_{\min}}{\xi_{\mathrm{ref}}-\xi_{\min}}\right)^2 \cdot \frac{\ln\left(\frac{\xi-\xi_{\min}}{\xi_{\max}-\xi_{\min}}\right)}{\ln\left(\frac{\xi_{\mathrm{ref}}-\xi_{\min}}{\xi_{\max}-\xi_{\min}}\right)}, \quad (15)$$

where χ_{ref} is the scalar dissipation rate at a reference value of normalized enthalpy, here $\xi_{\mathrm{ref}} = 0.5$, and $\xi_{\min}$ and $\xi_{\max}$ are minimum and maximum enthalpies in the CFD field, which are not necessarily equivalent to $\Theta_{\min}$ and $\Theta_{\max}$.

The local value of the conditional scalar dissipation rate at the representative normalized enthalpy is also obtained from an expression analogous to the mixture fraction formulation [13], given by

$$\widetilde{\chi}_{\mathrm{ref}} = \frac{\widetilde{\chi}\ \xi_{\mathrm{ref}}^2 \ln(\xi_{\mathrm{ref}})}{\int_0^1 \xi^2 \ln(\xi)\tilde{P}(\xi;\mathbf{x},t)\,d\xi}, \quad (16)$$

where $\tilde{P}(\xi;\mathbf{x},t)$ is the probability density function, taken here to be a Gaussian function. The flamelet code requires a characteristic value for the scalar dissipation rate conditioned on the representative normalized enthalpy for the entire cylinder. A surface average of this value is calculated by converting the surface integrals to volume integrals following [16] as

$$\widehat{\chi_{\mathrm{ref}}} = \frac{\int_V \bar{\rho}(\mathbf{x})\widetilde{\chi}_{\mathrm{ref}}^{3/2}(\mathbf{x})\ \tilde{P}(\xi;\mathbf{x},t)\,dV'}{\int_V \bar{\rho}(\mathbf{x})\widetilde{\chi}_{\mathrm{ref}}^{1/2}(\mathbf{x})\ \tilde{P}(\xi;\mathbf{x},t)\,dV'}. \quad (17)$$

RESULTS

Simulations were conducted in this study for the operating conditions of two experimental cases of Murase and Hananda (2002). The results of three simulations will be discussed in this section. Both of the two experimental cases (T_o = 333 and 323 K) were simulated using the modeled flamelet equations (Eqs. 11 & 12). In order to quantify the effects of diffusion in enthalpy space a third simulation was conducted for the case of T_o = 333 K, but with the scalar dissipation rate, χ_ξ, set to zero. This third case represents zero-diffusion in enthalpy-space, corresponding to a series of homogeneous reactors or an idealized multizone model. The ignition times for both the experiments [6] and the simulations, as a function of initial gas temperature are given in Table 1. The two main simulations predict the ignition timing with very good accuracy showing differences of 0.4 and 0.9 ms for T_o = 333 and T_o = 323 K respectively. The magnitude of this error is within 2%.

CASE	T_o	$\tau_{\mathrm{exp,ign}}$	$\tau_{\mathrm{sim,ign}}$	$\tau_{\mathrm{sim\ no\ dif,ign}}$
1	333 K	57.6 ms	57.2 ms	64.2 ms
2	323 K	60.4 ms	59.5 ms	-

Table 1: Ignition timing for two initial temperatures (at Φ = 0.4) from experiments [6], simulations with enthalpy-based flamelet Eqs. (11) & (12), and simulations without the diffusion term, $\chi_\xi = 0$.

The computed temperature as a function of normalized enthalpy, ξ, is plotted in Fig. 2 for the T_o = 333 K case. The region most affected by wall heat loss is located at $\xi = 0$ while the mixture at $\xi = 1$ is not affected by wall heat loss. The simulation predicts that the regions not affected by the wall heat loss ignite first ($\xi = 1$) at approximately 56 ms.

From Fig. 2 we can observe that due to diffusion in enthalpy space, an ignition front propagates in ξ-space from

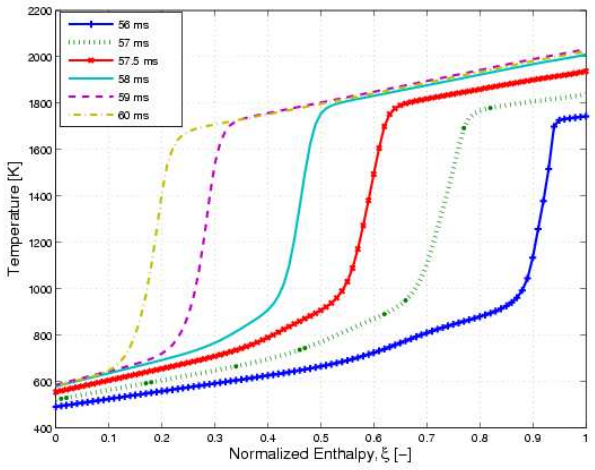

Figure 2: Flamelet solution of temperature as a function of normalized total enthalpy, ξ, for various times for simulation with initial temperature of 333 K.

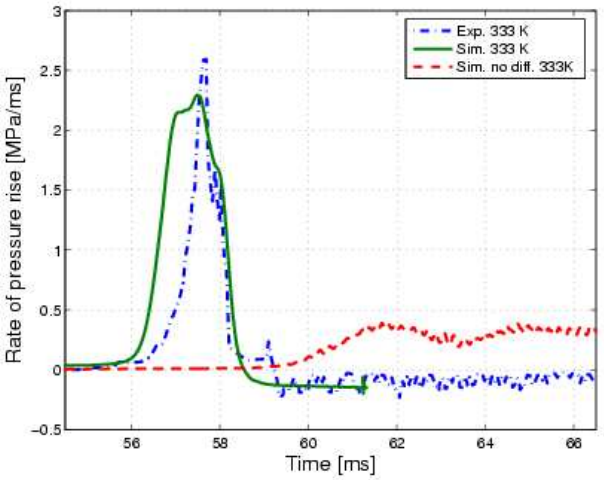

Figure 3: Rate of pressure rise vs. time [MPa/ms] for case 1, $T_o = 333$ K, for both experiment and simulations.

large enthalpies, $\xi = 1$, to small enthalpies, $\xi = 0$. In this study, thermal diffusion in enthalpy-space is modeled as the second and third terms in Eq. (12),

$$\mathsf{Diff} = \frac{\rho\chi_\xi}{2}\frac{\partial^2 T}{\partial\xi^2} + \frac{\rho\chi_\xi}{2C_p}\frac{\partial T}{\partial\xi}\left(\frac{\partial C_p}{\partial\xi} + \sum_i^{\mathrm{N}} c_{p,i}\frac{\partial Y_i}{\partial\xi}\right). \quad (18)$$

Because of the large enthalpy gradients and the exponential temperature dependence on reaction rates, this term cannot be neglected. As given in Table 1, when the thermal diffusion term is omitted, the simulation predicts an ignition time of 64.2 ms, which substantially over predicts the experimentally obtained value of 57.6 ms. This should be contrasted with the much better 57.2 ms prediction in the case that the thermal diffusion term is included.

In Fig. 3 we show the rate of pressure rise for the experiment ($T_o = 333$ K) and the two case 1 simulations as function of time. The simulation with the diffusion term predicts the magnitude of the maximum rate of pressure rise, duration of combustion, and the timing of ignition reasonably well. Conversely, the simulation without the diffusion term under predicts the maximum rate of pressure rise, over predicts the duration of combustion, and significantly over predicts the timing of ignition.

In order to quantify the effects of the various terms in Eq. (12), convection, pressure, and chemical source terms defined as,

$$\mathsf{Conv} = \frac{\partial Y_i}{\partial H}\left(\rho\frac{\partial H}{\partial t} + \rho v_j\frac{\partial H}{\partial x_j}\right), \quad (19)$$

$$\mathsf{Pres} = \frac{1}{C_p}\left(\frac{\partial p}{\partial t} - \dot{q}_{\Delta h}\right), \quad (20)$$

$$\mathsf{Chem} = -\frac{\rho}{C_p}\sum_i^{\mathrm{N}} h_i\dot{\omega}_i \quad (21)$$

are normalized by the total rate of change in temperature and plotted in Fig. 4 as a function of ξ during ignition, at a time of 57.5 ms. As shown in the figure, the chemical source term is largest contribution at the ignition front ($\xi \approx 0.62$). However, the diffusion term is the dominating term in the unburnt gas just ahead of the front ($0.50 < \xi < 0.55$), acting to increase the temperature of those gases. The effect of diffusion in enthalpy-space is to increase the propagation velocity of the front, and thereby advance ignition timing and decrease the total combustion duration. However, diffusion is less important in regions far from the front. The coupling between these unburnt gases ($0.0 < \xi < 0.4$) and the front is realized through the pressure term. This pressure term models the increase in pressure associated with volumetric expansion of gas during combustion.

Figure 5 shows the spatial distribution of the Favre averaged enthalpy, temperature, normalized enthalpy, and velocity fields for the case with an initial temperature of 333 K. The top figures are just before ignition (57 ms), the middle figures are during ignition (57.5 ms), and the bottom plot is just after ignition (58 ms). Since these plots correspond to temperature curves in Fig. 2, the affects of the propagation of the ignition front in ξ-space has on the evolution of the mean temperature field in physical space can be seen in Fig. 5. This evolution of the mean temperature field is qualitatively consistent with photographs of light emissions for the experimental case reported in Ref. [6].

CONCLUSION

An enthalpy-based flamelet model for HCCI-like ignition was derived and applied to a rapid compression machine operated under HCCI-like conditions. Transport between regions affected by wall heat loss and less affected regions

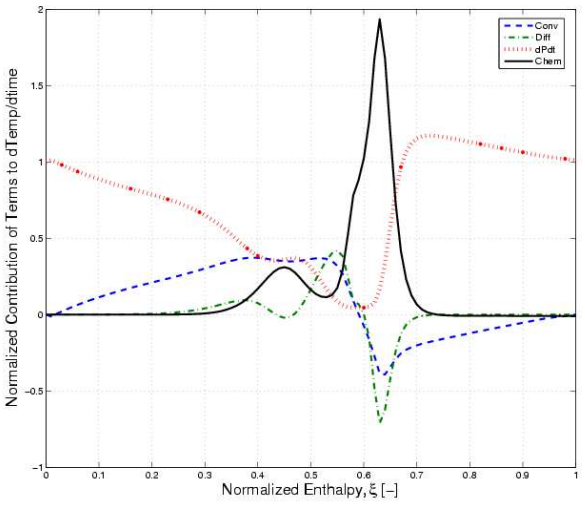

Figure 4: Convection, diffusion, pressure, and chemical source terms in flamelet equation for temperature (Eq. 12), normalized by total time rate of change in temperature as a function of normalized enthalpy, during ignition, 57.5 ms.

was appears as diffusion in a normalized enthalpy space. The model correctly predicts ignition timing trends initial temperatures. This model predicts the propagation of an ignition front in enthalpy space. A simulation with the diffusion term set to zero was not able to predict ignition characteristics adequately. The effect of the various terms in the flamelet equations was quantified. In the ignition front, the chemical source term is dominant. The diffusion term was shown to be dominant in the immediate surroundings of the front, while the pressure term was the dominant term far from the front. The results of this study indicate that for HCCI-like combustion with large enthalpy gradients and a fully premixed charge, diffusion in enthalpy-space affects combustion characteristics and can be modeled using enthalpy-based flamelets. This model is not, however, able of capturing the affects of mixture composition inhomogeneities that are present in Direct Injection HCCI and to some extent in all HCCI engines. To account for such inhomogeneities a second dimension in the flamelet equations accounting for the mixture composition inhomogeneities will have to be introduced. Such a two-dimensional flamelet model and its application to a simulation of an HCCI engine is the focus of our future work.

ACKNOWLEDGMENTS

This work has been funded in part by Robert Bosch Corporation's Research and Technology Center in Palo Alto, California. The authors would like to thank the RTC Flameless Combustion group: Dr. Aleksandar Kojić, Dr. Jasim Ahmed, and Dr. Sungbae Park for helpful discussions and comments. The authors would also like to thank Perrine Pepiot for her help with the reduction of the chemical mechanism.

APPENDIX

In order to simplify the numeric solution of these equations, the enthalpy field is normalized. The normalization uses variables, $\Theta_{\min}$ and $\Theta_{\max}$, that represent the minimum and maximum possible enthalpies in the system. They are defined as

$$\Theta_{\min}(\tau) = H_{\min,o} + \int_{\tau_o}^{\tau} \frac{1}{\rho}\left(\frac{\partial p}{\partial t} - \dot{q}_{\Delta h} - \frac{dh}{dt}\Big|_{\text{wall}}\right) dt \quad (22)$$

$$\Theta_{\max}(\tau) = H_{\max,o} + \int_{\tau_o}^{\tau} \frac{1}{\rho}\left(\frac{\partial p}{\partial t} - \dot{q}_{\Delta h}\right) dt \quad (23)$$

where $\frac{dh}{dt}\big|_{\text{wall}}$ represents the maximum temporal rate of change of enthalpy caused by wall heat losses. This term is applied only to the minimum possible enthalpy, as all other enthalpies will be affected by wall heat loss through the diffusion and convection terms in enthalpy-space as given by Eqs. (11) & (12). The enthalpy field can now be normalized by the maximum and minimum enthalpys as

$$\xi = \frac{H - \Theta_{\min}(\tau)}{\Theta_{\max}(\tau) - \Theta_{\min}(\tau)} = \frac{H - \Theta_{\min}(\tau)}{\Delta\Theta(\tau)}. \quad (24)$$

Now a coordinate transformation is performed to transform the flamelet equations from H and τ space into ξ and $\tau^\star$ space. The transformation rules are as follows,

$$\frac{\partial}{\partial \tau} = \frac{\partial \tau^\star}{\partial \tau}\frac{\partial}{\partial \tau^\star} + \frac{\partial \xi}{\partial \tau}\frac{\partial}{\partial \xi} = \frac{\partial}{\partial \tau^\star} + \frac{\partial \xi}{\partial \tau}\frac{\partial}{\partial \xi} \quad (25)$$

$$\frac{\partial}{\partial H} = \frac{\partial \tau^\star}{\partial H}\frac{\partial}{\partial \tau^\star} + \frac{\partial \xi}{\partial H}\frac{\partial}{\partial \xi} = \frac{\partial \xi}{\partial H}\frac{\partial}{\partial \xi} \quad (26)$$

Differentiating Eq. (24) with respect to H and τ gives

$$\begin{aligned}\frac{\partial \xi}{\partial \tau} &= \frac{1}{\Delta\Theta(\tau)}\left(-\frac{\partial \Theta_0(\tau)}{\partial \tau} - \xi\frac{\partial \Delta\Theta(\tau)}{\partial \tau}\right) \\ &= -\frac{1-\xi}{\rho_0 \Delta\Theta(\tau)}\left(\frac{\partial p}{\partial t} - \dot{q}_{\Delta h,0} - \frac{dh}{dt}\Big|_{\text{wall}}\right) \\ &\quad -\frac{\xi}{\rho_1 \Delta\Theta(\tau)}\left(\frac{\partial p}{\partial t}\right) \quad (27)\end{aligned}$$

$$\frac{\partial \xi}{\partial H} = \frac{1}{\Delta\Theta(\tau)}. \quad (28)$$

Defining new variables λ, λ_0 and λ_1 as

$$\lambda(\xi, \tau^\star) = \frac{1}{\rho(\xi,\tau^\star)\Delta\Theta(\tau^\star)}\left(\frac{\partial p(\tau^\star)}{\partial t} - \dot{q}_{\Delta h}(\xi,\tau^\star)\right) \quad (29)$$

$$\begin{aligned}\lambda_0(\tau^\star) &= \frac{1}{\rho_0(\tau^\star)\Delta\Theta(\tau^\star)}\left(\frac{\partial p(\tau^\star)}{\partial t}\right) \quad (30)\\ &\quad - \frac{1}{\rho_0(\tau^\star)\Delta\Theta(\tau^\star)}\left(\frac{dh}{dt}\Big|_{\text{wall}} + \dot{q}_{\Delta h,0}(\tau^\star)\right)\end{aligned}$$

$$\lambda_1(\tau^\star) = \frac{1}{\rho_1(\tau^\star)\Delta\Theta(\tau^\star)}\left(\frac{\partial p(\tau^\star)}{\partial t}\right), \quad (31)$$

and substituting Eqs. (27)-(31) into Eqs. (25)-(26) predicts the coordinate transformation rules in final form

$$\frac{\partial}{\partial \tau} = \frac{\partial}{\partial \tau^\star} - \Big((1-\xi)\cdot\lambda_0(\tau^\star) + \xi\cdot\lambda_1(\tau^\star)\Big)\frac{\partial}{\partial \xi} \quad (32)$$

$$\frac{\partial}{\partial H} = \frac{1}{\Delta\Theta(\tau^\star)}\frac{\partial}{\partial \xi}. \quad (33)$$

In order to simplify this transformation, a new variable representing a convective velocity in ξ-space, is introduced as

$$v_\xi = \Big(\lambda - (1-\xi)\cdot\lambda_0 - \xi\cdot\lambda_1\Big). \quad (34)$$

Applying the transformation rules in Eqs. (32) & (33) to the enthalpy space flamelet equations given by Eq. (9) results in the normalized enthalpy-based flamelet equations in final form as given by Eqs. (11) & (12).

References

[1] Christensen, M., et al., SAE Technical Paper, No. 2002-01-2864, 2002.

[2] Dec, J., SAE Paper 2002-01-1309, 2002.

[3] Aceves, S.M., Flowers, D.L., Westbrook, C.K., Smith, J.R., Pitz, W.J., Dibble, R., Christensen, M., Johansson, B., SAE paper 2000-01-0327, 2000.

[4] Kong, S.C. and Reitz, R.D., Proc. Combust. Inst., 29, 663-669. 2002

[5] Cook, D.J., Pepiot, P., and Pitsch, H., The Proceedings of The 4th Joint Meeting of U.S. Sections of The Combust. Inst., 2005.

[6] Murase, H., and Hanada, K., SAE Paper 2002-01-2867, 2002.

[7] Curran, H. J., Gaffuri, P., Pitz, W. J., and Westbrook, C. K., Combustion and Flame 114:149-177, 1998.

[8] Pepiot, P., and Pitsch, H., The Proceedings of The 4th Joint Meeting of U.S. Sections of The Combust. Inst., 2005.

[9] Hawkes, E.R., Sankaran, R., Chen, J.H., and Im, H.G., The Proceedings of The 4th Joint Meeting of U.S. Sections of The Combust. Inst., 2005.

[10] Burcat, A., Scheller, K., and Lifshitz, A., Combust. Flame, 16:29-33, 1971.

[11] Pitsch, H., Barths, H., and Peters, N., SAE Paper 962057, 103-117, 1996.

[12] Peters, N., *Turbulent Combustion*, pp. 30-169, Cambridge University Press, 2000.

[13] Hergart, C., Peters, N., Transactions of the ASME, 124, 1042-1052, 2002.

[14] Barths, H., Hasse, C., Bikas, G., Peters, N., Proc. Combust. Inst., 28, 1161-1168, 2000.

[15] Jones, W.P., Whitelaw, J.H., Combust. and Flame, 48, 1, 1-26, 1982.

[16] Pitsch, H, Ph.D. thesis, Rheinisch-Westfälische Technische Hochschule, Institut für Technische Mechanisk, Feb. 1998.

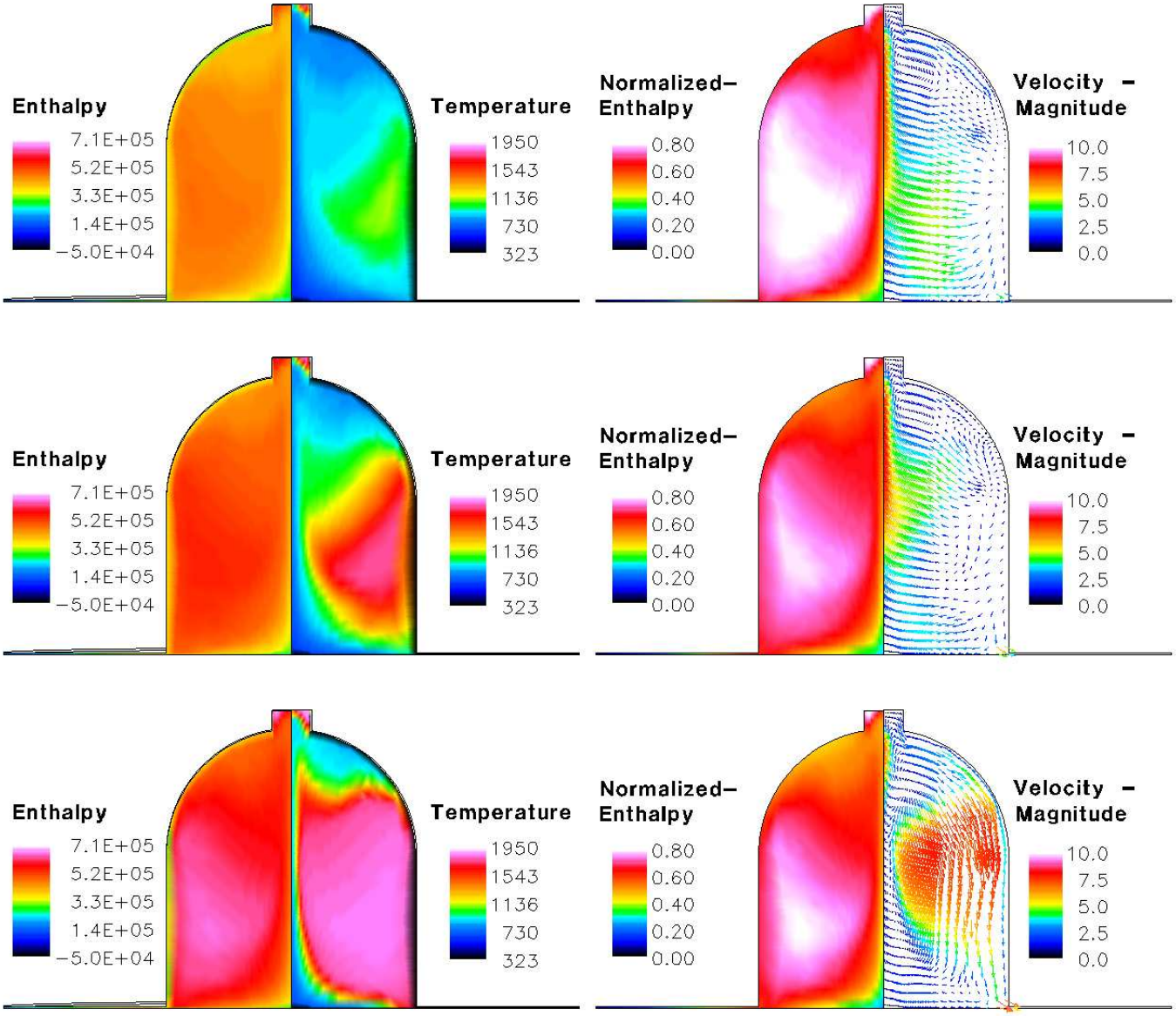

Figure 5: Contours of Farve averaged enthalpy, temperature, normalized enthalpy, and velocity fields for the case with an initial temperature of 333 K. The top figures are just before ignition, while the bottom figures are just after ignition.